Available online at www.sciencedirect.com
ScienceDirect
Journal of Magnetic Resonance 184 (2007) 114–129
JMR Journal of Magnetic Resonance
www.elsevier.com/locate/jmr

Encoding of diffusion and T_1 in the CPMG echo shape: Single-shot D and T_1 measurements in grossly inhomogeneous fields

Martin D. Hürlimann *

Schlumberger-Doll Research, Old Quarry Road, Ridgefield, CT 06877, USA

Received 10 August 2006; revised 20 September 2006
Available online 17 October 2006

Abstract

We present a new approach of NMR measurements in the presence of grossly inhomogeneous fields where information is encoded in the echo shape of CPMG trains. The method is based on sequences that consist of an initial encoding sequence that generates echoes with contributions from at least two different coherence pathways that are then both refocused many times by a long string of closely spaced identical pulses. The generated echoes quickly assume an asymptotic shape that encodes the information of interest. High signal-to-noise ratios can be achieved by averaging the large number of echoes. We demonstrate this approach with different implementations of the measurements of longitudinal relaxation time, T_1, and diffusion coefficient, D. It is shown that the method can be used for novel single-shot measurements.

Keywords: Inhomogeneous fields; Diffusion; Relaxation; CPMG; Ex situ NMR

1. Introduction

The development of new NMR techniques to characterize large samples is currently an active field [1–3]. In these applications, the samples frequently do not fit inside standard superconducting magnets and require one-sided magnet systems. This poses special experimental challenges: the magnetic field across the sample is necessarily inhomogeneous and the signal-to-noise ratio is intrinsically low.

A natural scale for inhomogeneities in B_0 is the amplitude of the rf field, B_1. In grossly inhomogeneous fields when the field inhomogeneities in B_0 exceed B_1, all rf pulses are slice-selective and the nutation angles vary significantly across the sample. The spectra of the NMR signal are then primarily controlled by the excitation bandwidth, proportional to B_1, and the value of T_2^* is of the order of the pulse duration. This implies that standard NMR spectroscopy, used in the vast majority of NMR experiments, cannot be used to encode chemical or spatial information in the signal spectrum. A number of techniques [4,1,5,6] have been developed to extend spectroscopy to cases where the inhomogeneity in the static field is larger than the line splittings, but still small compared to B_1.

Despite this drawback, NMR in grossly inhomogeneous fields has found a number of significant applications, particularly in the field of oil-well logging [3]. Until recently, these measurements have been based predominantly on the Carr–Purcell–Meiboom–Gill (CPMG) sequence [7,8]. In this case, the essential information is contained in the amplitudes of the echo. In particular, the initial amplitude and the decay time of the amplitudes are routinely used to infer important material properties such as porosity and pore size.

The basic CPMG measurement has been successfully extended to multi-dimensional measurements in grossly inhomogeneous fields [9]. For this purpose, the initial 90° pulse is replaced by an initial pulse sequence that is systematically varied to change the sensitivity to the quantity of interest. This is then followed by a long string of closely spaced refocusing pulses. Examples include the measurements of D–T_2 distribution functions [9], T_1–T_2

* Fax: +1 203 438 3819.
E-mail address: hurlimann@slb.com

1090-7807/$ - see front matter © 2006 Elsevier Inc. All rights reserved.
doi:10.1016/j.jmr.2006.09.021

distribution functions [9], flow propagators [10,11], and 3d imaging [12].

In all these measurements, information is encoded into the amplitudes of echoes. Here we show that it is possible to encode information directly into the shape of the CPMG echoes. We demonstrate that this allows single-shot measurements of diffusion and T_1.

In the next section, we review the relevant spin dynamics in grossly inhomogeneous fields and discuss different encodings of information into the CPMG echo shapes. We present several implementations of the new approach for T_1 measurements in Section 4 and for diffusion measurements in Section 5.

2. Spin dynamics in grossly inhomogeneous fields

We first briefly review the spin dynamics of CPMG-like sequences in grossly inhomogeneous fields. The standard CPMG sequence consists of an initial nominal 90° pulse that generates transverse magnetization. This magnetization is then periodically refocused by a long string of closely spaced 180° pulses. The performance of this sequence in grossly inhomogeneous fields when the range of Larmor frequencies, $\Delta\omega_0$, is much larger than the rf nutation frequency, ω_1, has been analyzed by a number of authors [13–15]. In grossly inhomogeneous fields, the spectrum of echoes quickly approaches an asymptotic form, and the magnetization of the kth echo can be written as [14]

$$\vec{M}_k(\omega_0) = (\vec{M}_{90}(\omega_0)\cdot\hat{n}(\omega_0))\hat{n}(\omega_0)\ \exp\{-kt_E/T_{2,\mathrm{eff}}\} \qquad (1)$$

Here $\vec{M}_{90}$ is the magnetization after the initial 90° pulse, $\hat{n}$ is the axis of the effective rotation of a refocusing cycle, t_E is the echo spacing, and $T_{2,\mathrm{eff}}$ is the relaxation time. The explicit dependence of $\vec{M}_{90}$ and $\hat{n}$ on ω_0 and ω_1 can be found in [14]. The asymptotic spectrum of the echoes is given by $S(\omega_0) = (\vec{M}_{90}(\omega_0)\cdot\hat{n}(\omega_0))\hat{n}_\perp(\omega_0)$. On resonance, $S(\omega_0 = 0) = M_0$, the thermal equilibrium magnetization, and the width of $S(\omega_0)$ is of the order of ω_1. The asymptotic echo shape in the time domain, $S(t)$, is simply the Fourier transform of $S(\omega_0)$. Here t is the time from the nominal echo center and is bounded by $[-t_E/2, t_E/2]$. In the time domain, the signal at a total time $T = kt_E + t$ can then be written as:

$$M(T = kt_E + t) = S(t)\exp\{-kt_E/T_{2,\mathrm{eff}}\} \qquad (2)$$

This expression is valid after the first few echoes when the neglected terms in Eq. (1) have averaged out to a high degree [14]. Eq. (2) shows that it is most efficient to use $S(t)$ as matched filter to extract echo amplitudes from the experimental data.

Note that in the CPMG sequence, the repeated refocusing serves two distinct roles. First, many echoes can be averaged to obtain the echo shape $S(t)$. This helps to overcome the intrinsically small signal-to-noise ratio in grossly inhomogeneous fields. Second, the time dependence of the echo amplitudes allows the measurement of the relaxation time $T_{2,\mathrm{eff}}$.

The formulation Eq. (1) makes it evident that only the component of the initial magnetization $\vec{M}_{90}$ along the axis $\hat{n}$ is refocused. This is a general feature of CPMG-like sequences in grossly inhomogeneous fields and still holds when the pulses are replaced by composite pulses [16]. This analysis can be generalized to two-dimensional experiments where the initial 90° pulse is replaced by a preparation sequence such as an inversion–recovery sequence ($180° - t_1 - 90°$) or a stimulated echo sequence ($90° - \delta - 90° - T_d - 90° - \delta$) to encode T_1 or diffusion information [9]. In this case, Eq. (1) is modified by replacing $\vec{M}_{90}$ by the magnetization after the initial preparation period, $\vec{M}_A$:

$$\vec{M}_k = (\vec{M}_A\cdot\hat{n})\hat{n}\exp\{-kt_E/T_{2,\mathrm{eff}}\} \qquad (3)$$

To calculate M_A and its dependence on diffusion, T_1 or other parameters, it is necessary to divide the evolutions into different coherence pathways [17,18]. For any coherence pathway i, the response in grossly inhomogeneous fields can be factorized into a spectrum $s_i(\omega_0)$ and an amplitude $a_i(D, T_1, \ldots)$ [19]. The spectrum $s_i(\omega_0)$ depends only on the rf pulses. The effects of diffusion, relaxation, flow or pulsed field gradients perpendicular to the static gradient are uniform across the spectrum and are described by the amplitude a_i, which depends on the duration of the time intervals between the rf pulses. We can therefore write the spectrum $(\vec{M}_A\cdot\hat{n})\hat{n}$ in Eq. (3) as a sum over the different coherence pathways

$$S(\omega_0) = (\vec{M}_A\cdot\hat{n})\hat{n} = \sum_{i=1}^{N} s_i(\omega_0)a_i(D, T_1, \ldots). \qquad (4)$$

In the standard implementation of multi-dimensional NMR in grossly inhomogeneous fields [9], a single coherence pathway is selected. Changing the timing in the preparation period systematically results in a variation of the overall echo amplitudes of the CPMG echoes and is analogous to the encoding of the second dimension in conventional multi-dimensional NMR [18].

Here we propose to choose preparation sequences such that at least two coherence pathways contribute to the signal. Since different coherence pathways have in general different sensitivities on diffusion or T_1, the spectrum (Eq. (4)) or echo shape of the CPMG echoes now depends on these parameters. In this case, the information of the second dimension is not only encoded in the relative echo amplitudes, but also in the echo shapes. Note that with this modification, the shapes remain invariant in an echo train after the first few echoes. It is therefore still possible to average many echoes to achieve good statistics. The crucial point of the new method is that the measurement of the echo shape of a single CPMG train already allows the extraction of the parameter of interest.

To optimize this single-shot approach, preparation pulse sequences must be chosen with significant contributions from different coherence pathways that exhibit greatly different sensitivities to the parameter of interest and

simultaneously have echo shapes that are as orthogonal to each other as possible.

We demonstrate different experimental implementations of this idea for T_1 in Section 4 and for diffusion measurements in Section 5. Additional applications are discussed in Section 6.

3. Experimental

To demonstrate the feasibility of the new concept, we conducted experiments on a sample of doped water with a relaxation time $T_1 = T_2 = 114$ ms in the fringefield outside a superconducting magnet. The rf frequency was set at 1.764 MHz and the static gradient was $g = 132$ mT/m. We typically acquired 1000–2000 echoes in the CPMG train. The diameter of the sample was 38 mm. This is much larger than the typical slice thickness $2\omega_1/(\gamma g) \simeq 0.7$ mm. Therefore, we can neglect to first order the finite sample size along the gradient direction.

4. T_1 measurements

4.1. Standard inversion–recovery sequence

The concept of encoding T_1 in the echo shape can be demonstrated with the standard inversion–recovery sequence, combined with CPMG detection. The sequence is shown in Fig. 1A. Details of the spin dynamics for this sequence in grossly inhomogeneous fields have been discussed in [19]. After the recovery time t_1, at the time of the 90° pulse, the magnetization has components from two different coherence pathways that are usually referred to as "decay" and "recovery" components [20–22].

Following the notation of Ref. [19] the spectrum of the echoes, $S(\omega_0)$, after the first few refocusing pulses is given by

$$S(\omega_0) = s_1(\omega_0)\exp\{-t_1/T_1\} + s_2(\omega_0)(1 - \exp\{-t_1/T_1\}), \quad (5)$$

where the spectra of the individual coherence pathways are given by:

$$s_1(\omega_0) = M_0 \Im m\left(\Lambda^{(3)}_{+1,-1}\Lambda^{(2)}_{-1,0}\Lambda^{(1)}_{0,0}e^{-i\omega_0 t_{180}/\pi}\right)n_y^2 \quad (6)$$

$$s_2(\omega_0) = M_0 \Im m\left(\Lambda^{(3)}_{+1,-1}\Lambda^{(2)}_{-1,0}e^{-i\omega_0 t_{180}/\pi}\right)n_y^2 \quad (7)$$

Here M_0 is the thermal equilibrium magnetization, $\Lambda^{(k)}_{i,j}$ are transition probabilities for the kth pulse between the three different magnetization components (M_{+1}, M_{-1}, M_0), given explicitly in [19], n_y is the y-component of the effective rotation axis for the refocusing cycle [14], and $t_{180} = \pi/\omega_1$ is the duration of the nominal 180° pulse. To maximize the signal, the pulse spacing between the 90° pulse and the first 180° refocusing pulse should be reduced from half the echo spacing by t_{180}/π [23]. This reduction is reflected in Eqs. (6) and (7) by the extra phase shifts of $\exp\{-i\omega_0 t_{180}/\pi\}$.

Based on the expressions (6) and (7) we can calculate the echo shapes due to the decay and recovery components. For an extended sample along the gradient direction, the echo shapes in the time domain of the two components are then simply the Fourier transforms of Eqs. (6) and (7). The theoretical results are shown in Fig. 2.

The echo shapes during the CPMG detection are a T_1-weighted sum of the two contributions:

$$S(t) = s_1(t)\exp\{-t_1/T_1\} + s_2(t)(1 - \exp\{-t_1/T_1\}) \quad (8)$$

This is confirmed by the experimental echo shapes shown in Fig. 3. In the experiments, we varied the recovery time t_1 logarithmically between 1 ms and 10 s. The signal from

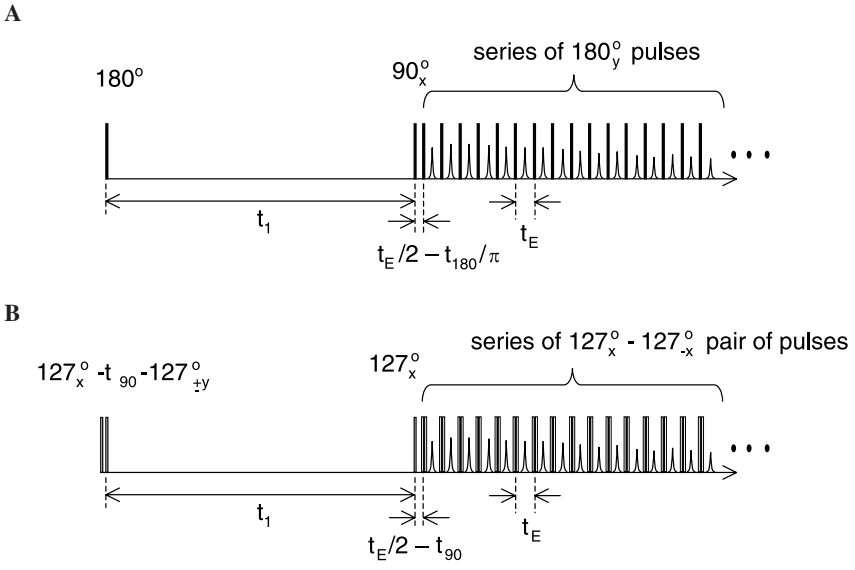

Fig. 1. Examples of pulse sequences used to encode T_1 information in echo shape: (A) standard inversion–recovery–CPMG sequence using nominal 180° and 90° pulses. (B) New modified inversion–recovery–CPMG sequence. It is based on the composite inversion pulse $127^\circ_x - t_{90} - 127^\circ_{\pm y}$ that produces a predominantly anti-symmetric inversion profile, followed by a string of $127^\circ_x - 127^\circ_{-x}$ pulses that completely refocus magnetization off-resonance at $\omega_0 = \pm\omega_1$. Here t_1 is the recovery time, t_E is the echo spacing, and t_{90} and t_{180} are the durations of nominal 90° and 180° pulses, respectively.

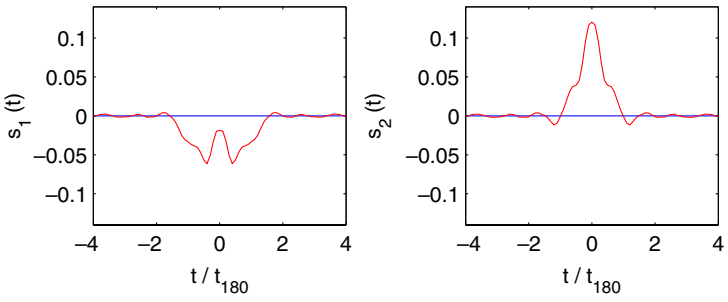

Fig. 2. Calculated echo shapes for the decaying (left) and recovering (right) coherence pathway for the standard inversion–recovery sequence with CPMG detection (Fig. 1A) in grossly inhomogeneous fields. Both echo shapes have only contributions in phase with the 180° refocusing pulses.

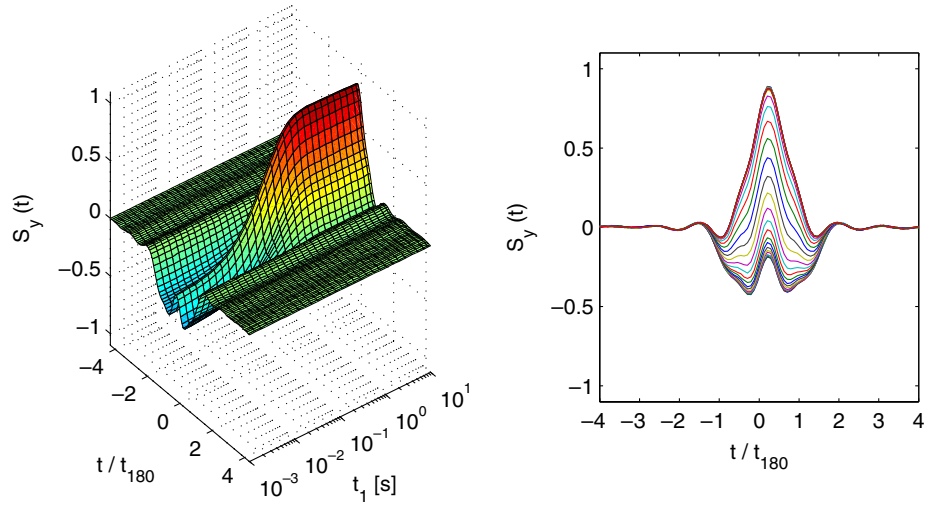

Fig. 3. Standard inversion–recovery–CPMG detection: experimental echo shapes of the signal in phase with the refocusing pulses for different recovery times t_1 in the range of 1 ms to 10 s. The echo shapes were obtained by averaging the 10th to the 110th echo shape. In these measurements, the pulse durations were $t_{180} = 2t_{90} = 24$ μs and the echo spacing was $t_E = 384$ μs.

the 10th to the 110th echo was averaged to obtain the echo shapes displayed. For recovery times $t_1 \ll T_1 = 114$ ms the measured echo shapes coincide with the theoretical shape $s_1(t)$, whereas in the other limit, $t_1 \gg T_1$, the echo shapes approach $s_2(t)$. This confirms the sensitivity of the echo shape to the T_1 relaxation time.

For any value of recovery time t_1, the experimental echo shapes can be decomposed into a weighted sum of $s_1(t)$ and $s_2(t)$: $S_y(t) = a_1 s_1(t) + a_2 s_2(t)$. Given the echo shapes $s_1(t)$ and $s_2(t)$, the amplitudes a_1 and a_2 can be extracted from a measured echo shape $S(t)$ by:

$$a_1 = \frac{(s_1 \cdot S)(s_2 \cdot s_2) - (s_1 \cdot s_2)(s_2 \cdot S)}{(s_1 \cdot s_1)(s_2 \cdot s_2) - (s_1 \cdot s_2)(s_2 \cdot s_1)}$$
$$a_2 = \frac{(s_2 \cdot S)(s_1 \cdot s_1) - (s_2 \cdot s_1)(s_1 \cdot S)}{(s_1 \cdot s_1)(s_2 \cdot s_2) - (s_1 \cdot s_2)(s_2 \cdot s_1 r)}, \quad (9)$$

where $(s_1 \cdot S) = \int dt\, s_1^*(t) S(t)$ and similar other terms are integrals over the acquisition window.

We have used this procedure to extract the amplitudes a_1 and a_2 from every echo shape shown in Fig. 3. The results are displayed in Fig. 4 as a function of t_1. They closely follow the predictions of Eq. (8), i.e. the amplitudes have a simple exponential dependence on t_1/T_1. A quantitative comparison is given below in Section 4.3.

The expressions (6) and (7) for the spectra implicitly assume a constant B_1 field and a flat B_0 field distribution corresponding to a constant gradient. However, it is straightforward to extend the approach to more general field inhomogeneities. In this case, the expressions (6) and (7) can be interpreted as sensitivity functions $s_i(\omega_0, \omega_1)$ that depend on both ω_0 and ω_1. For field inhomogeneities characterized by a $B_0 - B_1$ distribution function $f(\omega_0, \omega_1)$, the observed spectra are then given by $s_i(\omega_0) = \int d\omega_1 f(\omega_0, \omega_1)\, s_i(\omega_0, \omega_1)$. The rest of the analysis is unaffected. The practical implementation of the method in a specific sensor requires the knowledge of the spectra $s_i(\omega_0)$. They can be calculated from the given field distribution function $f(\omega_0, \omega_1)$. However, it is often more efficient to determine the individual spectra s_i experimentally using $t_1 \ll T_1$ and $t_1 \gg T_1$, respectively.

4.2. Improved pulse sequence with composite pulses

The new method relies on the analysis of the measured echo shapes. In practice, it is essential to use the CPMG detection to obtain a sufficient signal-to-noise ratio, as it

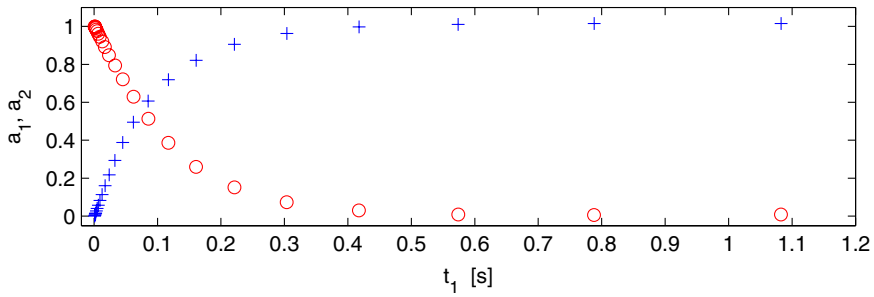

Fig. 4. Experimental results of the amplitudes of the decaying (○) and recovering (+) coherence pathways versus recovery time t_1 for the standard inversion–recovery–CPMG sequence. The amplitudes were extracted from the echo shapes shown in Fig. 3.

allows the averaging of many echoes. To make this method as robust as possible, the echo shapes corresponding to the two coherence pathways should be as large as possible and as orthogonal to each other as possible. It is evident from Fig. 2 that for the standard inversion–recovery–CPMG sequence, there is a large overlap ($s_1 \cdot s_2$) between the two echo shapes. We demonstrate next that the orthogonality can be greatly improved with the use of composite pulses.

We set the goal to generate the contributions of the two coherence pathways 90° out of phase to each other. When CPMG detection is used in grossly inhomogeneous fields, this is impossible in the frequency domain, as the refocusing pulses can only refocus a single component of the transverse magnetization [14]. However, it is possible in the time domain by generating contributions of the decaying and recovering coherence pathways that are anti-symmetric and symmetric in terms of ω_0, respectively. For samples extended along the gradient direction, the two signals will then form out-of-phase to each other in the time domain. Based on Eq. (6), this requires an anti-symmetric inversion pulse.

The standard 180° pulse generates a symmetric inversion profile, as shown in Fig. 5A. A well-known method to generate an anti-symmetric profile is the half-adiabatic-fast-passage, Fig. 5B. The main drawback of this approach is that the relatively long duration of the frequency sweep adds uncertainty to the exact definition of the recovery time t_1.

Alternatively, an anti-symmetric inversion profile can be approximated with the novel sequence

$$127^{\circ}_{x} - t_{90} - 127^{\circ}_{\pm y}. \tag{10}$$

Here two nominal 127° pulses are separated by a time of free precession of duration t_{90}, the width of a nominal 90° pulse. The duration of the 127° pulses is $\sqrt{2}$ times longer than t_{90}. As a consequence, at offset frequencies $\omega_0 = \pm\omega_1$, the 127°_{x} pulse acts as a 180° pulse around the $(\hat{x} \pm \hat{z})/\sqrt{2}$ axis. The resulting longitudinal magnetization of the new inversion pulse (10) is shown in Fig. 5C. This composite pulse generates an inversion profile with a large anti-symmetric component for frequency offset less than $2\omega_1$. In particular, at $\omega_0 = \pm\omega_1$, the resulting longitudinal magnetization is $\pm M_0$, i.e. complete inversion at $-\omega_1$ and fully restored magnetization at $+\omega_1$.

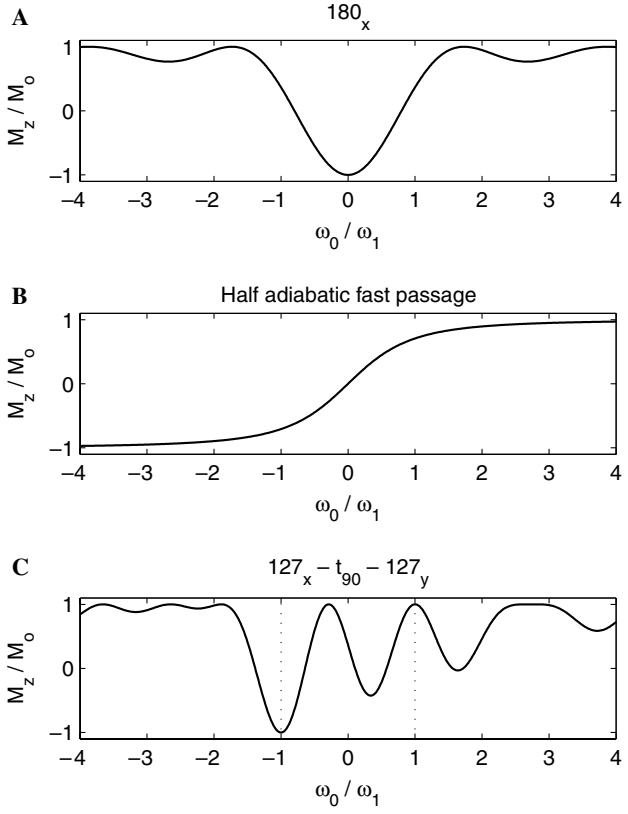

Fig. 5. Longitudinal magnetization after inversion pulse. (A) standard 180° inversion pulse, (B) half adiabatic fast passage, (C) new composite pulse $127^{\circ}_{x} - t_{90} - 127^{\circ}_{y}$.

To refocus this magnetization, we combine this inversion sequence with the previously described [16] off-resonance CPMG sequence $127_x - (t_E/2 - t_{90}) - (127_x\, 127_{-x} - t_E)^N$ to obtain the improved inversion–recovery sequence, shown in Fig. 1B

$$\left(127^{\circ}_{x} - t_{90} - 127^{\circ}_{\pm y}\right) - t_1 - (127_x - (t_E/2 - t_{90}) - (127_x 127_{-x} - t_E)^N). \tag{11}$$

The calculated response for the two coherence pathways is shown in Fig. 6. Both spectra have only contributions in phase with the axis of the effective rotation describing the refocusing cycle. For the composite pulse 127_x127_{-x}, this is the y-axis [16]. At offset frequencies $\pm\omega_1$, the magnitudes

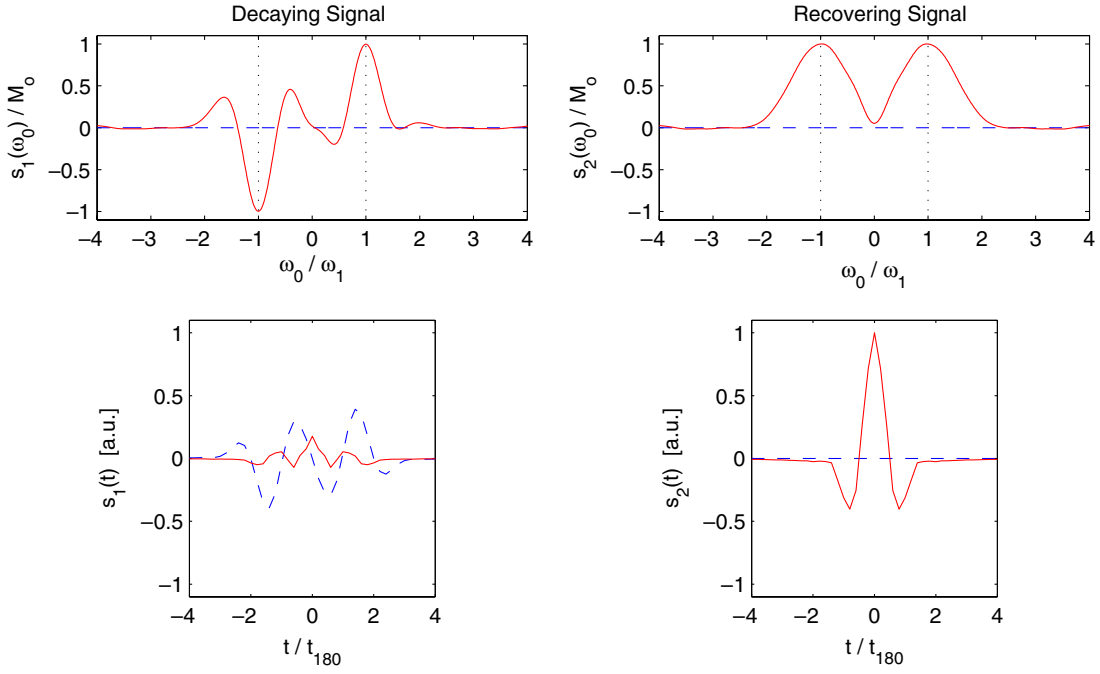

Fig. 6. Calculated spectra (top) and echo shapes (bottom) of the decaying (left) and the recovering (right) coherence pathways for the pulse sequence shown in Fig. 1B. These spectra have been convoluted with $\sin(\omega_0 t_E/2)/(\omega_0 t_E/2)$ to account for the fact that the signal for each echo can only be detected for a duration less than t_E. In-phase contributions are shown as solid lines, out-of-phase contributions as dashed lines.

$|s_i(\pm\omega_1)| = M_0$, i.e. the maximum possible magnetizations are obtained for both coherence pathways.

The spectrum of the recovering coherence pathway corresponds to the CPMG-like response discussed in [16]. With the phases of pulses and timings shown in Fig. 1B, the spectrum of the decaying coherence pathways is predominately anti-symmetric with respect to ω_0, whereas the spectrum of the recovering coherence pathway is symmetric with respect to ω_0. As a result, the echo shapes in the time domain have only in-phase components for the recovering coherence pathway and predominantly out-of-phase components for the decaying coherence pathway. The smaller in-phase component in the decaying coherence pathway is caused by the residual symmetric component in the spectrum of this coherence pathway.

Experimental results for the modified sequence are shown in Fig. 7. The echo shapes were extracted by averaging the signal from the 10th to 110th echo. The shapes agree well with the theoretical results of Fig. 6. For small t_1, the signal is dominated by the out-of-phase component of the decaying coherence pathways. As t_1 increases, the amplitude of the out-of-phase echo shape decreases, while the in-phase signal increases. The ratio of out-of-phase to in-phase signal is directly related to the relative size of the recovery time t_1 to the relaxation time T_1.

The decomposition of the experimental echo shapes into the components of the two coherence pathways is still described by Eq. (8). In Fig. 8 we show the extracted amplitudes for the two coherence pathways. There is excellent agreement with the expected exponential dependence on t_1/T_1.

As noted before, the modified sequence does not generate a perfectly anti-symmetric longitudinal magnetization after the inversion pulse. As a consequence, the decaying coherence pathways generates a small in-phase component. It is possible to extract the purely anti-symmetric signal of this coherence pathways by phase cycling: Changing the phase of the second pulse from $+y$ to $-y$ effectively inverts the frequency axis, i.e. it only affects the anti-symmetric signal. If the signals generated by the two sequences are subtracted from each other, only the anti-symmetric, out-of-phase signal contributes. It results in an exact subtraction of the recovering signal over the whole spectrum.

The new composite pulse sequence drastically improves the orthogonality of the two signals $s_1(t)$ and $s_2(t)$. Quantitatively, the normalized cross product $|(s_1 \cdot s_2)/\sqrt{(s_1 \cdot s_1)(s_2 \cdot s_2)}| = 0.15$ for the modified sequence, compared to *0.62* for the standard sequence. In addition, the signal power of the CPMG echoes is increased with the new sequence, as demonstrated in Fig. 9. With the standard sequence, there is substantial cancellation between the signals of the two coherence pathways when the recovery time is close to $\log 2 T_1$. This leads to a pronounced dip in signal power of the CPMG echoes. This problem is avoided with the new sequence because the two contributions are predominately out-of-phase and do not cancel.

The current experiments were performed with a fairly uniform B_1 field. The results in [16] show that the off-resonance pulses are rather robust to deviations in B_1 and can be used even in situations with significant B_1 inhomogeneities.

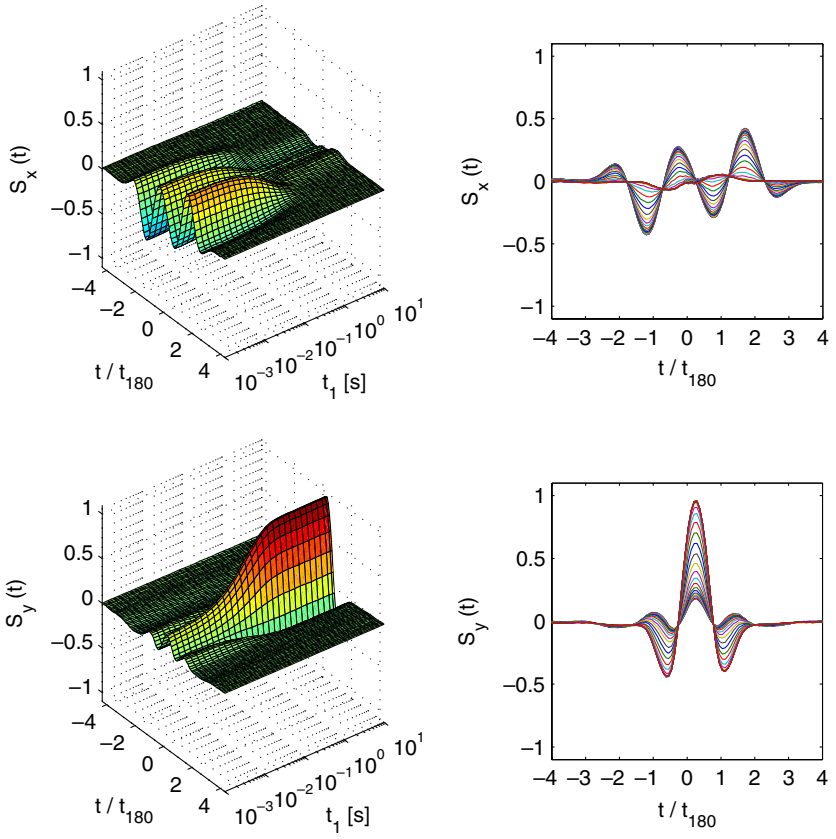

Fig. 7. Experimental results of echo shapes versus recovery time t_1 for the modified pulse sequence of Fig. 1B. The out-of-phase components are shown on top, the in-phase components are shown at the bottom.

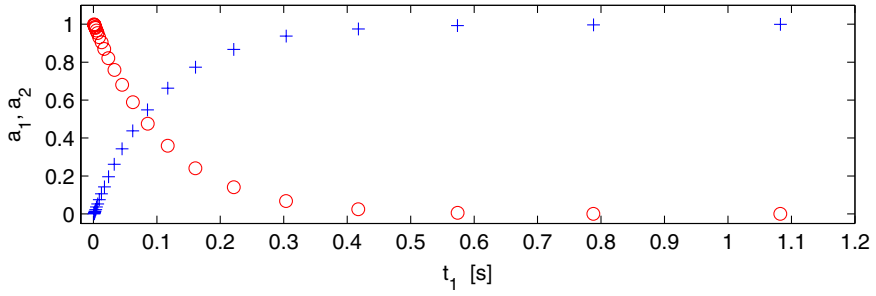

Fig. 8. The experimental results of the amplitudes of the decaying (○) and recovering (+) coherence pathways versus recovery time t_1 for the modified inversion–recovery–CPMG sequence, Fig. 1B show the expected exponential dependence on t_1/T_1. The amplitudes were extracted from the echo shapes shown in Fig. 7 based on Eq. (9).

4.3. Implication for single-shot measurement of T_1

The results above demonstrate that the echo shape of the CPMG echoes depends on the longitudinal relaxation time. It should therefore be possible to extract T_1 from the echo shape in a single-scan measurement. For any given inversion–recovery pulse sequence, we can calculate the expected echo shapes $s_i(t)$ for the two coherence pathways and then decompose the echoes into these two components. The relative amplitude of these components is directly related to the longitudinal relaxation time:

$$\frac{a_1}{a_1 + a_2} = \exp\{-t_1/T_1\}. \tag{12}$$

This general relationship is shown in Fig. 10 by the solid line and compared with the experimental results for the two sequences. The experimental results agree well with the prediction of Eq. (12). This demonstrates that it is possible to extract T_1 from the echo shape in a single-scan measurement. For good sensitivity, Fig. 10 shows that the recovery time t_1 should be chosen such that T_1/t_1 is in the range of about 0.4 to 10, i.e. t_1 should be in the range between $0.1T_1$ and $2.5T_1$. If the T_1 relaxation is characterized by a distribution $f(T_1)$ rather than a single relaxation

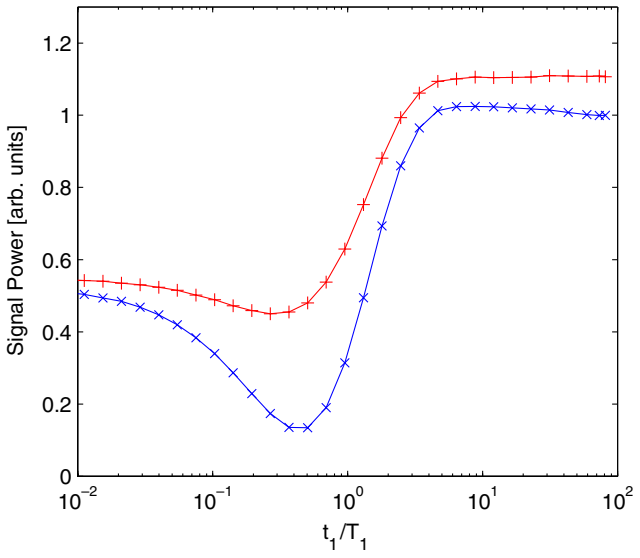

Fig. 9. Signal power of the CPMG detected signal versus the ratio of recovery time and longitudinal relaxation time, t_1/T_1. The × symbols show experimental results using the standard inversion-recovery-CPMG sequence, and the + signs show results with the modified sequence. For all values of t_1/T_1, the modified sequence generates larger signals and avoids the pronounced dip for $t_1 \approx \log 2 T_1$.

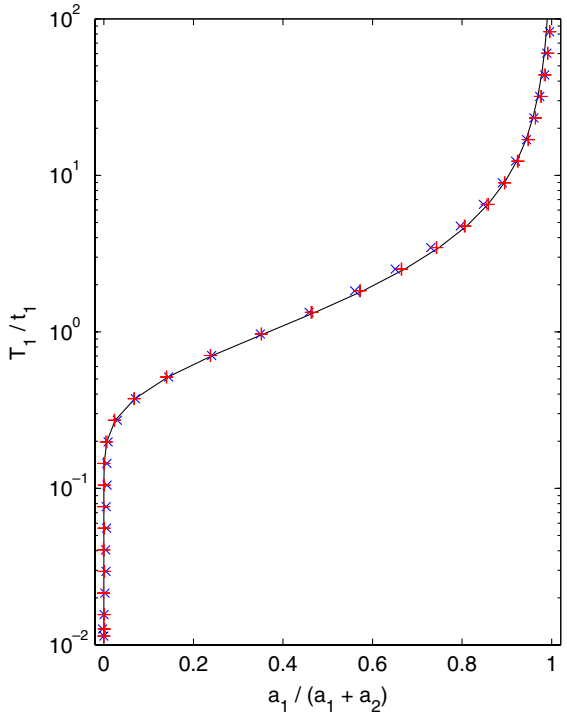

Fig. 10. Relationship between the longitudinal relaxation time, T_1 and relative size of the amplitudes of the decaying and recovering coherence pathway. The solid line shows Eq. (12), × shows experimental results using the standard inversion–recovery–CPMG sequence, on + shows results with the modified sequence using off-resonance pulses.

time, then the t_1 dependence of the amplitudes is more complicated. In a single-shot measurement, the amplitude ratio Eq. (12) is then related to the following quantity:

$$\frac{a_1}{a_1+a_2} = \frac{\int dT_1 f(T_1)\exp\{-t_1/T_1\}}{\int dT_1 f(T_1)}. \tag{13}$$

It is worthwhile to compare this new approach with previous signal-scan T_1 methods [24,25] that were designed for more homogeneous fields. A number of these schemes are derived from the so-called 'triplet method' [26], where the recovering longitudinal magnetization is stroboscopically monitored by briefly converting it into transverse magnetization, detect it, and then restore it back to longitudinal magnetization. This approach cannot be easily extended to grossly inhomogeneous fields, as off-resonance effects prevent complete conversion of longitudinal into transverse magnetization and back. As a result, the measured relaxation rates become a mixture of T_1^{-1} and T_2^{-1}. More recently, Loening et al. [27] have introduced another single-scan approach that is based on the standard 2d inversion–recovery sequence, where the second dimension is encoded in the spatial dimension using pulsed field gradients. This allows the simultaneous encoding of the second dimension in different slices of the sample and therefore reduces the measurement time of the 2d experiment to that of a 1d experiment. In principle, this approach can be generalized to grossly inhomogeneous fields by encoding different recovery times with multiple rf frequencies that differ by more than ω_1. The main experimental challenges of such an approach are the required fast frequency switching and broadband detection.

5. Diffusion encoding in echo shape

5.1. Principles

The general approach of encoding NMR information in the echo shape can also be applied to diffusion measurements. If more than two pulses are applied in grossly inhomogeneous fields, multiple echoes form that have different sensitivities to diffusion in the static background gradient [28,29,19,30]. For our purpose, it is essential that at least some of the echoes form at nearly identical times so that CPMG detection can be employed. A simple example of such a pulse sequence is shown in Fig. 11(A). It consists of a CPMG sequence where the first two echo spacings have been increased to encode diffusion information [9]. After the second 180° pulse, the direct echo and stimulated echo coherence pathways generate an echo at the same time that is then refocused by the subsequent long series of 180° pulses. The signal is maximized if the first pulse spacing is reduced from $t_E/2$ to $t_E/2 - t_{180}/\pi$, as indicated in Fig. 11(A). A detailed analysis of the spin dynamics of this sequence can be found in [31].

The echo shape measured with the CPMG detection, $S(t)$, is a weighted superposition of the echo shape $s_{de}(t)$ due to the direct echo coherence pathway and $s_{se}(t)$ due to the stimulated echo coherence pathway. The weights depend on the diffusion and relaxation parameters of the sample, but the echo shapes $s_{de}(t)$ and $s_{se}(t)$ are

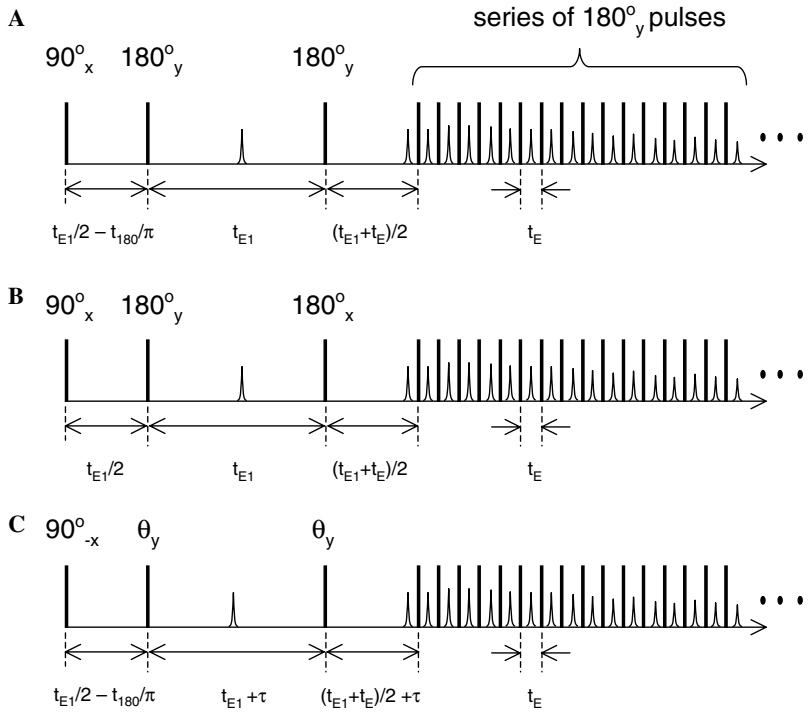

Fig. 11. Examples of diffusion editing sequences that consist of an initial three pulse sequence to encode diffusion information, followed by CPMG detection through a long series of 180° pulses. (A): standard sequence used for two-dimensional measurements of $D - T_2$ distribution functions [9,31]. Both direct echo and stimulated echo coherence pathways contribute to the signal. However, it is difficult to separate the two contributions from the echo shape generated by this sequence. The modified sequences (B) and (C) greatly improve this and are suitable for single-shot application. In (B), the phase of the second 180° pulse is shifted from y to x. As a result, the signals of the two coherence pathways form out-of-phase to each other. In (C), the second echo spacing is increased by τ. In this implementation, the echoes in the CPMG detection have a central peak due to the direct echo and two side peaks due to stimulated echo shifted by $\pm\tau$. The nominal flip angle θ controls the relative weights of the two coherence pathways.

independent of these parameters and depend only on the rf pulses.

$$S(t) = s_{\mathrm{de}}(t)\exp\left\{-\frac{1}{6}\gamma^2 g^2 t_{E1}^3 D\right\}\mathrm{e}^{-2t_{E1}/T_2} + s_{\mathrm{se}}(t) \times \exp\left\{-\frac{1}{3}\gamma^2 g^2 t_{E1}^3 D\right\}\mathrm{e}^{-t_{E1}\left(\frac{1}{T_1}+\frac{1}{T_2}\right)}. \quad (14)$$

Here g is the magnetic field gradient, D is the diffusion coefficient, and t_{E1} is the echo spacing for the first two echoes.

The echo shapes $s_{\mathrm{de}}(t)$ and $s_{\mathrm{se}}(t)$ can be calculated following the procedure given in [19] and the results are shown in Fig. 12(A).

In this case, both coherence pathways form echoes centered in the acquisition window that are difficult to separate clearly from each other. A more reliable separation of the two contributing coherence pathways can be achieved with slight modifications of the basic pulse sequence. This is illustrated in Figs. 12(B) and (C) with two different modifications that separate the contributions either by phase (B) or in the time domain (C).

With the pulse sequence shown in Fig. 11(B), the signals of the two contributions form out-of-phase to each other, as shown in Fig. 12(B). This is analogous to the approach used in Section 4.2 for T_1 encoding. This type of separation is accomplished by changing the phase of one of the first two 180° pulses by 90°. In addition, the timing of the first two pulses has to be slightly adjusted. In sequence (B), the optimized pulse spacing of the first two pulses used in Sequence (A) maximizes the contribution of the direct echo, but minimizes the contribution of the stimulated echo. As a consequence, it is better to set the first pulse spacing to $t_E/2$, which greatly increases the stimulated echo contribution and only modestly decreases the direct echo signal.

In the second example, shown as sequence (C) in Fig. 11, the two contributions are separated directly in the time domain by increasing the second echo spacing by a small amount, τ. The stimulated echo then forms a duration τ earlier than the direct echo [15,30]. With the timing as shown in Fig. 11(C), the asymptotic echoes in the CPMG detection consist of a central peak due to the direct echo and two symmetric satellite peaks due to stimulated echo that are shifted by $\pm\tau$. This is shown in Fig. 12(C). The duration of τ has to be large enough to separate the two contributions, i.e. larger than t_{180}, but small enough so that the shifted peaks still lie within the detection window, i.e. $\tau < t_E/2$. The nominal flip angle θ controls the relative weights of the two coherence pathways.

5.2. Diffusion encoding by phase separation

We first present tests of the modified sequence shown in Fig. 11(B) on a sample of doped water. The initial echo

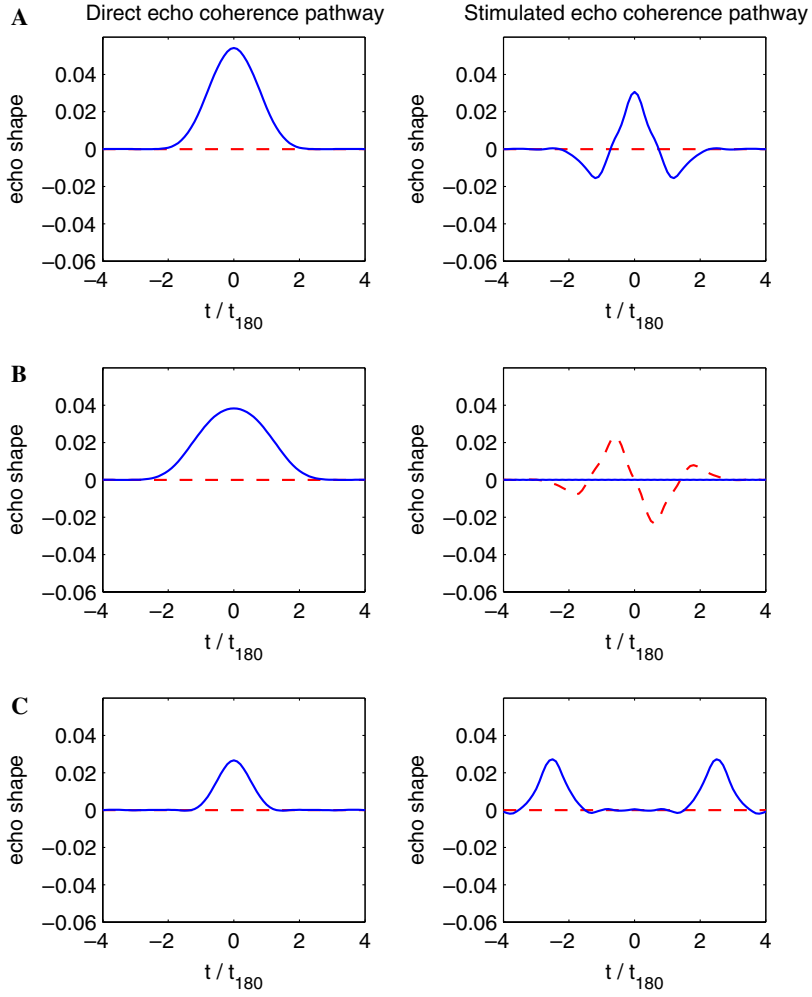

Fig. 12. Calculated echo shapes for the direct echo (left) and stimulated echo coherence pathway (right), respectively for three different pulse sequences shown in Fig. 11. The in-phase signal is shown as solid line, the out-of-phase signal as dashed line. For sequence (A) the two contributions strongly overlap. With (B), the contributions from the stimulated echo form out of phase with respect to those from the direct echo. With (C), the two contributions are separated in time. In this calculation, we assumed $\theta = 98°$ and $\tau = 2.5t_{180}$.

spacing t_{E1} was systematically increased in 32 steps to a maximum value of 17.1 ms. In all cases, the CPMG detection consisted of 2000 echoes that were acquired with an echo spacing of $t_E = 424$ μs. The durations of the nominal 90° and 180° pulses were $t_{90} = 24$ μs and $t_{180} = 48$ μs.

In Fig. 13 we show results for five different values of $\gamma^2 g^2 t_{E1}^3 D$. The left-hand side shows the echo shapes during the CPMG detection. They were extracted from the acquired data by averaging the shapes of the 100th to 300th echo. In agreement with the theoretical expectation shown in Fig. 12B, there are both sizeable in-phase and out-of-phase signals. The in-phase signals are symmetric and generated by the direct echo coherence pathway, while the out-of-phase signals are anti-symmetric and generated by the stimulated echo coherence pathways. As the initial echo spacings are increased, diffusion becomes more important and preferentially reduces the out-of-phase component. For each echo, we extracted the amplitudes of the two components, using as matched filters the expected echo shapes in the absence of diffusion. The results are shown on the right hand side of Fig. 13 versus the time after the initial 90° pulse. The results confirm the general form of Eq. (2), valid for sufficiently short echo spacing t_E: within a CPMG train, the echo shapes $S(t)$ remain unchanged and the amplitudes of all components decay with the same relaxation time. The solid black lines are fits to single exponential decays. We find identical relaxation times $T_{2,\text{eff}} = 114$ ms for all measurements.

The amplitudes of the first few echoes show a characteristic transient effect, similar to that observed with the standard CPMG sequence [14]. This is well understood and is caused by imperfect averaging of the magnetization perpendicular to the net axis $\hat{n}$. The results show that these terms only contribute noticeably to the first few echoes, for later echoes the asymptotic expression given in Eq. (3) is an excellent approximation.

The fitted amplitudes, extrapolated to zero time, are shown in Fig. 14. Both the amplitudes of the in-phase and the out-of-phase components decay exponentially as a function of the dimensionless diffusion coefficient,

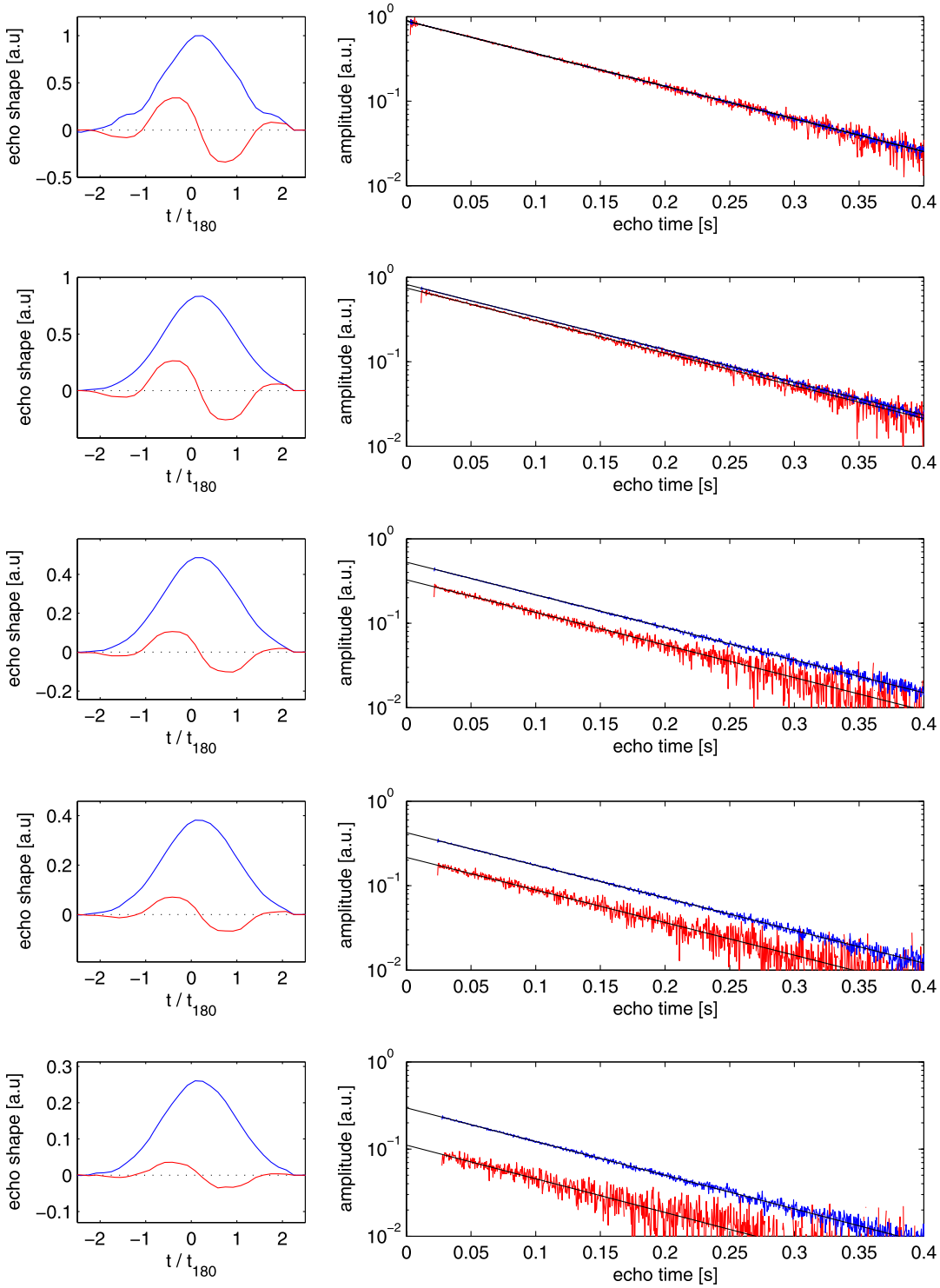

Fig. 13. Experimental results for phase encoding of diffusion information, using the pulse sequence shown in Fig. 11B. The five rows show results for different initial pulse spacings, $\gamma^2 g^2 t_{E1}^3 D = 0.01$, 0.4, 3.1, 4.4, and 6.5, respectively. The panels on the left display in-phase and out-of-phase components of the echo shapes $S(t)$. On the right, the extracted amplitudes of the in-phase and out-of-phase components are shown versus the total time after the initial 90° pulse. The solid lines are fits to a single exponential decay with $T_{2,\mathrm{eff}} = 114$ ms.

$\gamma^2 g^2 t_{E1}^3 D$, but with exponents that differ by a factor of 2. This confirms that the in-phase and the out-of-phase components are associated with the direct echo or stimulated echo coherence pathways, respectively. In addition, there is excellent agreement between the experimental results in Fig. 14 and the theoretical prediction of Eq. (14) shown as solid lines.

There are no adjustable parameters in the comparison between experiments and theory in Fig. 14. At the lowest levels, the measured amplitudes of the out-of-phase

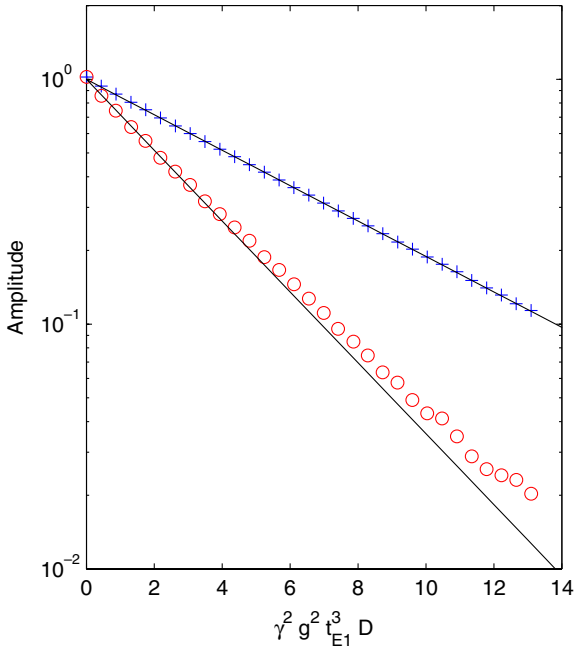

Fig. 14. Fitted initial amplitudes of the in-phase echo signal (+) and out-of-phase echo signal (○) versus the dimensionless diffusion coefficient, $\gamma^2 g^2 t_{E1}^3 D$, for phase encoding of the diffusion information. The solid lines show the expected dependence for direct echo coherence pathway (top) and stimulated echo coherence pathway (bottom) based on Eq. (14).

component are somewhat above the theoretical results. This is likely caused by small mixing of the direct echo coherence pathway into the out-of-phase signal. Possible causes of such mixing include asymmetries of the sample shape along the gradient, asymmetry in the frequency response of the NMR detection system, or imperfect tuning.

5.3. Diffusion encoding by time separation

We have also tested diffusion encoding by separating the contributions of the two coherence pathways temporally, using the sequence in Fig. 11(C). Here the durations of the nominal 90° and 180° pulses were $t_{90} = 12$ μs and $t_{180} = 24$ μs. The duration of the second and third pulse was set to 14 μs, corresponding to a nutation angle $\theta = 105°$ on resonance. The delay τ was set to 60 μs $= 2.5 t_{180}$. We have acquired data for 32 different initial echo spacing t_{E1} up to 17.1 ms. The CPMG detection consisted of 2000 echoes, acquired with an echo spacing of $t_E = 400$ μs.

Fig. 15 shows results obtained with this sequence. The echoes form in-phase, with a central peak and two symmetrical satellite peaks. With the values of the pulse duration chosen in the experiments, the amplitudes of the two satellite peaks and the central peak are almost identical when diffusion is not important. As the diffusion effect is increased, the satellite peaks due to the stimulated echo coherence pathways attenuates more than the central peak that is generated by the direct echo coherence pathways. Using the expected echo shapes for the two coherence pathways as matched filters, the amplitudes of the two components were extracted are displayed on the right hand side of Fig. 15. As expected, the relaxation time $T_{2,\mathrm{eff}} = 114$ ms during the CPMG train is identical to the value found in the previous implementation of Fig. 13.

The decay of the fitted amplitudes of the two contributions versus the dimensionless diffusion coefficient $\gamma^2 g^2 t_{E1}^3 D$ is shown in Fig. 16. The agreement with theory is excellent, even at low levels.

5.4. Implication for single-shot measurement of diffusion

In both implementations of diffusion encoding in the echo shape, the value of the diffusion coefficient can be already extracted from the measurement with a single value of t_{E1}. The results shown in Figs. 14 and 16 demonstrate that the ratio of the amplitudes of the two components is directly related to the diffusion coefficient. In Fig. 17, we compare the relationship between the dimensionless diffusion coefficient and the ratios of the measured amplitudes with the theoretical prediction

$$\gamma^2 g^2 t_{E1}^3 D = -6 \log(a_{se}/a_{de}). \tag{15}$$

With increasing values of t_{E1}, the ratio of the two amplitudes increases, but at the same time, the absolute amplitudes decrease. In situations with limited signal-to-noise ratio, it is best to optimize the absolute difference between the two amplitudes. In the case of the temporal separation of the two coherences, this will occur when $t_{E1}^3 \simeq (6 \log 2)/(\gamma^2 g^2 D)$.

Note that the ratio a_{se}/a_{de} is not affected by relaxation effects during the CPMG sequence. In our experiments, relaxation during the encoding sequence is also compensated for since $T_1 = T_2$ in our sample. In the more general case with $T_1 \neq T_2$, a correction term $t_{E,1}(1/T_2 - 1/T_1)$ has to be added to the left-hand side of Eq. (15).

It is possible to use more complicated pulse sequences that fully compensate for relaxation effects by choosing two coherence pathways that have identical relaxation, but different diffusion sensitivities. An example with a 4-pulse encoding sequence is the following sequence:

$$\Big[90^\circ_x - (t_{E1}/2 - t_{180}/\pi) - 90^\circ_y - t_{E1} - 90^\circ_x - (t_{E1} + \tau) \\ -90^\circ_y - (t_{E1}/2 + t_E/2 + \tau)\Big] - (180_y - t_E)^N. \tag{16}$$

The two direct echo coherence pathways $-+-+$ and $--++$ are only affected by T_2 and have therefore identical relaxation behavior, but they have different diffusion sensitivity. In the time domain, their contributions form in-phase with the 180° refocusing pulses as central and satellite peaks, respectively. The ratio of these amplitudes is therefore only a function of diffusion, and is independent of T_1 or T_2. The other coherence pathways are stimulated-echo-like with both T_1 and T_2 sensitivities and can be easily separated as they form contributions only in the out-of-phase channel. Note that this improved relaxation compensation comes at the price of lower overall signal amplitudes.

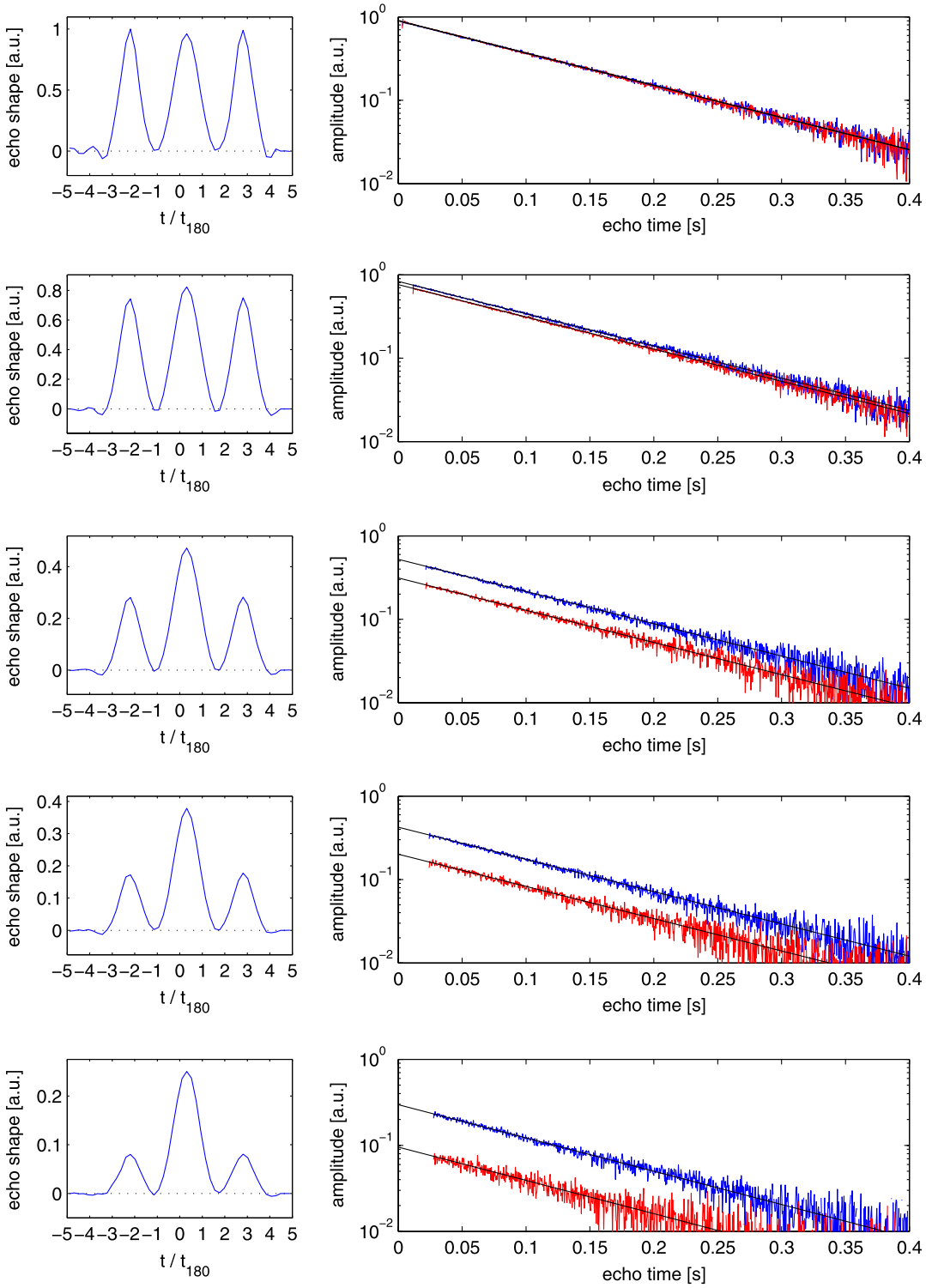

Fig. 15. Experimental results for encoding of diffusion information by time separation, using the pulse sequence shown in Fig. 11C. The five rows show results for different initial pulse spacings, $\gamma^2 g^2 t_{E1}^3 D = 0.01$, 0.4, 3.1, 4.5, and 6.7, respectively. The panels on the left display the in-phase components of the echo shapes $S(t)$. On the right, the extracted amplitudes of the central peak and the satellite peaks are shown versus the total time after the initial 90° pulse. The solid lines are fits to a single exponential decay with $T_{2,\mathrm{eff}} = 114$ ms.

6. Extension to other applications

The general approach underlying the single-shot T_1 and diffusion measurements demonstrated in this paper can be extended to other applications. An example is the use of the 'diffusion sequences' shown in Fig. 11 for the detection and quantification of flow or convection. The two coherence pathways have distinctly different sensitivities to flow. To

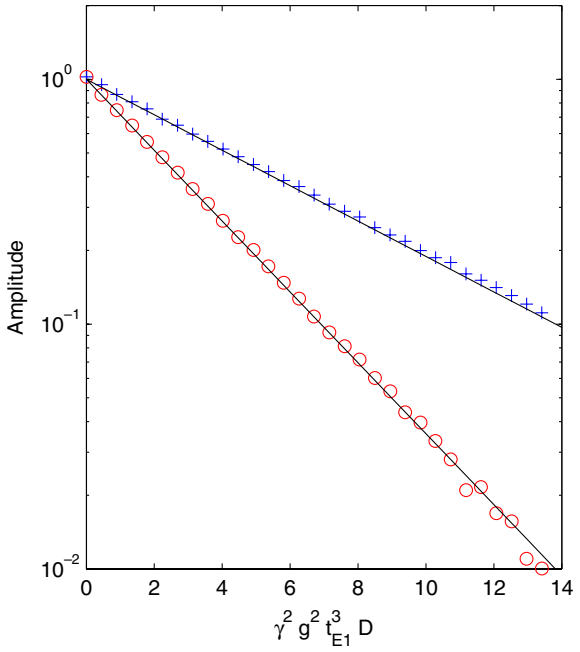

Fig. 16. Fitted initial amplitudes of the central peak (+) and the satellite peaks (○) versus the dimensionless diffusion coefficient, $\gamma^2 g^2 t_{E1}^3 D$, for diffusion encoding by temporal separation of the two contributions. The solid lines show the expected dependence for the direct echo coherence pathway (top) and stimulated echo coherence pathway (bottom).

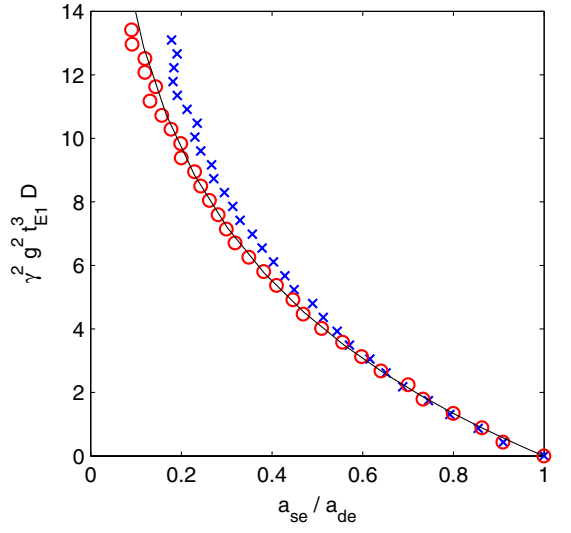

Fig. 17. Dimensionless diffusion coefficient versus signal amplitude ratio of the two coherence pathways. The symbols show experimental results (× using phase encoding, ○ using temporal separation) and the solid line is the theoretical prediction.

first order, the direct echo coherence pathway (corresponding to the second echo in a standard CPMG sequence) is unaffected by flow [7,32], whereas the in-phase amplitude of the stimulated echo coherence pathway is sensitive to the mean squared displacement of the spins with respect to the applied magnetic fields. When coherent motion dominates diffusion, this measurement provides a single-shot determination of the magnitude of the average flow velocity. This can be considered to be a combination of the flow measurement technique of Song and Scheven [33] with CPMG detection.

The technique can be also used to speed up imaging. Perlo et al. [12] demonstrated that it is possible to perform 3d imaging in grossly inhomogeneous fields, using pure phase encoding for the two directions perpendicular to the static gradient, combined with CPMG detection. Since the CPMG detection refocuses only the component of the magnetization that is in-phase with the 180° pulses, it requires two separate acquisitions with 180_x and 180_y refocusing pulses, respectively, to detect the critical phase information. This additional step doubles the already long acquisition time inherent with 2d phase encoding. In the limiting case of very high signal-to-noise ratio, the approach by Cho et al. [34] can be used where multiple echoes are generated that encode different values of $\vec{k}$. Here we consider the case when the signal-to-noise ratio of a single echo is insufficient and CPMG detection remains essential. In this case, the sequence shown in Fig. 18 can be used to encode two values of k simultaneously in the CPMG echoes. The direct echo coherence pathway, corresponding to the central echo peak is modulated with the wave vector $\vec{k}_2 - \vec{k}_1$, while the stimulated echo coherence pathways, leading to the satellite peaks, is modulated with $\vec{k}_1$. The amplitudes a_{de} and a_{se}, proportional to the echo peak amplitudes, are reduced by the wave vectors $\vec{k}_1$ and $\vec{k}_2$ as:

$$a_{de} = \frac{\int d\vec{x}_\perp e^{i(\vec{k}_2 - \vec{k}_1)\cdot\vec{x}_\perp} f(\vec{x}_\perp)}{\int d\vec{x}_\perp f(\vec{x}_\perp)} \tag{17}$$

$$a_{se} = \frac{\int d\vec{x}_\perp e^{\vec{k}_1\cdot\vec{x}_\perp} f(\vec{x}_\perp)}{\int d\vec{x}_\perp f(\vec{x}_\perp)}, \tag{18}$$

where $f(\vec{x}_\perp)$ is the spin density in the transverse direction $\vec{x}_\perp$. The sequence with 180°_y or 180°_x refocusing pulses then yield the real or imaginary part of a_{de} and a_{se}, respectively.

7. Conclusion

In standard NMR spectroscopy, the echo shape directly encodes the spectral information. When the homogeneity of the static B_0 field is degraded, this information gets lost. In this paper, we show that in the extreme limit of grossly inhomogeneous fields, it is possible to encode information such as diffusion or relaxation in the echo shapes.

This new approach is based on pulse sequences that excite at least two coherence pathways with different sensitivities to the quantity of interest and that refocus an echo in approximately the same time interval. It is advantageous to follow this encoding period with a long series of refocusing pulses. After an initial transient behavior, all subsequent echoes are expected to have an identical shape that depends on the encoded quantity. The detection efficiency can be greatly improved by averaging the echoes. The new technique is specific for applications in grossly inhomogeneous fields and does not have a direct analogue in fields of higher homogeneity.

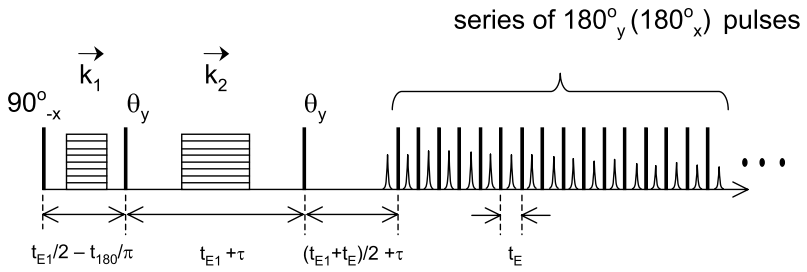

Fig. 18. Imaging sequence with CPMG detection for operation in grossly inhomogeneous fields. This is a modification of the diffusion sequence shown in Fig. 11C with pulsed field gradients. The CPMG echoes consist of a central peak with two satellite peaks, spaced τ apart. The central peak encodes information for $\vec{k}_2 - \vec{k}_1$, while the satellite peaks encode for $\vec{k}_1$. With 180°_y or 180°_x refocusing pulses, the real or imaginary part of a_{de} and a_{se} are acquired, respectively.

We have demonstrated that the new method is versatile and enables a range of novel measurements, including single-shot measurements of diffusion and T_1 measurements. In standard CPMG measurements, information is extracted from the initial amplitude and decay times of the echoes. In the new approach, additional information is contained in the shape of the echoes. In an alternative point-of-view, the signal is composed of a number of distinct components, corresponding to the different coherence pathways. By analyzing the shape of the echoes, each component can be detected separately. Therefore, different components are multiplexed on the same CPMG train.

We have demonstrated a number of experimental implementations of the new approach. The examples were chosen to illustrate different means to separate the components, including generating components that are out-of-phase to each other or shifted in time by small intervals.

References

[1] C.A. Meriles, D. Sakellariou, H. Heise, A.J. Moulé, A. Pines, Approach to high-resolution ex situ NMR spectroscopy, Science 293 (2001) 82–85.
[2] T.M. Brill, S. Ryu, R. Gaylor, J. Jundt, D.D. Griffin, Y.-Q. Song, P.N. Sen, M.D. Hürlimann, Nonresonant multiple spin echoes, Science 297 (2002) 369–372.
[3] R.L. Kleinberg. Encyclopedia of Nuclear Magnetic Resonance, vol. 8, chapter Well logging, John Wiley, Chichester, 1996, pp. 4960–4969.
[4] D.P. Weitekamp, J.R. Garbow, J.B. Murdoch, A. Pines, High-resolution NMR spectra in inhomogeneous magnetic fields: application of total spin coherence transfer echoes, J. Am. Chem. Soc. 103 (1981) 3578–3579.
[5] B. Shapira, L. Frydman, Spatial encoding and the acquistion of high-resolution NMR spectra in inhomogeneous magnetic fields, J. Am. Chem. Soc. 126 (2004) 7184–7185.
[6] J. Perlo, V. Demas, F. Casanova, C.A. Meriles, J. Reimer, A. Pines, B. Blümich, High-resolution NMR spectroscopy with a portable single-sided sensor, Science 308 (2005) 1279.
[7] H.Y. Carr, E.M. Purcell, Effects of diffusion on free precession in nuclear magnetic resonance experiments, Phys. Rev. 94 (1954) 630–638.
[8] S. Meiboom, D. Gill, Modified spin-echo method for measuring nuclear relaxation times, Rev. Sci. Instrum. 29 (1958) 688–691.
[9] M.D. Hürlimann, L. Venkataramanan, Quantitative measurement of two dimensional distribution functions of diffusion and relaxation in grossly inhomogeneous fields, J. Magn. Reson. 157 (2002) 31–42.
[10] F. Casanova, J. Perlo, B. Blümich, Velocity distributions remotely measured with a single-sided NMR sensor, J. Magn. Reson. 171 (2004) 124–130.
[11] U.M. Scheven, Stray field measurements of flow displacement distributions without pulsed field gradients, J. Magn. Reson. 174 (2005) 338–342.
[12] J. Perlo, F. Casanova, B. Blümich, 3d imaging with a single-sided sensor: an open tomograph, J. Magn. Reson. 166 (2004) 228–235.
[13] G. Goelman, M.G. Prammer, The CPMG pulse sequence in strong magnetic field gradients with applications to oil-well logging, J. Magn. Reson. A 113 (1995) 11–18.
[14] M.D. Hürlimann, D.D. Griffin, Spin dynamics of Carr–Purcell–Meiboom–Gill-like sequences in grossly inhomogeneous B_o and B_1 fields and application to NMR well logging, J. Magn. Reson. 143 (2000) 120–135.
[15] F. Bălibanu, K. Hailu, R. Eymael, D.E. Demco, B. Blümich, Nuclear magnetic resonance in inhomogeneous magnetic fields, J. Magn. Reson. 145 (2000) 246–258.
[16] M.D. Hürlimann, Carr–Purcell sequences with composite pulses, J. Magn. Reson. 152 (2001) 109–123.
[17] R. Kaiser, E. Bartholdi, R.R. Ernst, Diffusion and field-gradient effects in NMR Fourier spectroscopy, J. Chem. Phys. 60 (1974) 2966–2979.
[18] R.R. Ernst, G. Bodenhausen, A. Wokaun, Principles of Nuclear Magnetic Resonance in One and Two Dimensions, Clarendon Press, Oxford, 1987.
[19] M.D. Hürlimann, Diffusion and relaxation effects in general stray field NMR experiments, J. Magn. Reson. 148 (2001) 367–378.
[20] J.-J. Hsu, I.J. Lowe, Spin–lattice relaxation and a fast T_1-map acquisition method in MRI with transient-state magnetization, J. Magn. Reson. 169 (2004) 270–278.
[21] X.-P. Tang, K.C. Chartkunchand, Y. Wu, A novel nuclear spin–lattice relaxation filter for separating the free and absorbed water in a matrix of titanate nanotubes, Chem. Phys. Lett. 399 (2004) 456.
[22] E.E. Sigmund, N. Caudal, Y.Q. Song, Rapid T_1 measurement via decay-recovery decomposition: Applications in fringe field and distributed relaxation experiments, Solid State Nucl. Magn. Reson. 29 (2006) 232–241.
[23] M.D. Hürlimann, Optimization of timing in the Carr–Purcell–Meiboom–Gill sequence, Magn. Reson. Imag. 19 (2001) 375–378.
[24] A. Sezginer, R.L. Kleinberg, M. Fukuhara, L.L. Latour, Very rapid simultaneous measurement of nuclear magnetic resonance spin–lattice relaxation time and spin–spin relaxation time, J. Magn. Reson. 92 (1991) 504–527.
[25] P.B. Kingsley, Methods of measuring spin–lattice (T_1) relaxation times: an annotated bibliography, Concepts Magn. Reson. 11 (1999) 243–276.
[26] H.T. Edzes, An analysis of the use of pulse multiplets in the single scan determination of spin–lattice relaxation rates, J. Magn. Reson. 17 (1975) 301–313.

[27] N.M. Loening, M.J. Thrippleton, J. Keeler, R.G. Griffin, Single-scan longitudinal relaxation measurements in high-resolution NMR spectroscopy, J. Magn. Reson. 164 (2003) 321–328.
[28] E.L. Hahn, Spin echoes, Phys. Rev. 80 (1950) 580.
[29] S. Peled, C.-H. Tseng, A. Sodickson, R.W. Mair, R.L. Walsworth, D.G. Cory, Single-shot diffusion measurement, J. Magn. Reson. 140 (1999) 320–324.
[30] Y.-Q. Song, X. Tang, A one-shot method for measurement of diffusion, J. Magn. Reson. 170 (2004) 136–148.
[31] M.D. Hürlimann, L. Venkataramanan, C. Flaum, The diffusion-spin relaxation time distribution function as an experimental probe to characterize fluid mixtures in porous media, J. Chem. Phys. 117 (2002) 10223–10232.
[32] G.H. Sørland, J.G. Seland, J. Krane, H.W. Anthonsen, Improved convection compensating pulsed field gradient spin-echo and stimulated-echo methods, J. Magn. Reson. 142 (2000) 323–325.
[33] Y.Q. Song, U.M. Scheven, An NMR technique for rapid measurement of flow, J. Magn. Reson. 172 (2005) 31–35.
[34] H. Cho, L. Chavez, D.P. Madio, E.E. Sigmund, Y.-Q. Song, Fast imaging with the MMME sequence, J. Magn. Reson. 180 (2006) 18–28.